LBL-27360

Lawrence Berkeley Laboratory
UNIVERSITY OF CALIFORNIA

Materials & Chemical Sciences Division

Presented at the 91st Annual Meeting
of the American Ceramic Society
Indianapolis, IN, April 25, 1989, and
to be published in the Proceedings

Anisotropy of Grain Growth in Alumina

J. Rödel and A.M. Glaeser

September 1989

Prepared for the U.S. Department of Energy under Contract Number DE-AC03-76SF00098.

LBL--27360

DE90 009045

Anisotropy of Grain Growth in Alumina

Jürgen Rödel[*+]

and

Andreas M. Glaeser[*]

Department of Materials Science and Mineral Engineering
University of California and
Materials and Chemical Sciences Division
Lawrence Berkeley Laboratory
Berkeley, CA 94720

Abstract:

Grain growth in theoretically dense undoped and MgO-doped polycrystalline alumina was studied and average grain boundary migration rates were compared to those of a-plane and c-plane sapphire during migration into the same undoped and MgO-doped materials. The results are discussed in terms of a grain size dependent grain boundary mobility grain boundary energy product, $M_b\gamma_b$. The grain size dependencies of the $M_b\gamma_b$ products for seed and matrix grains differ. Seed orientation appears to affect the nature of solute-boundary interactions. The importance of grain boundary structure on migration characteristics is also indicated by a demonstration of twin formation enhanced grain growth. [Key words: alumina, sapphire, grain growth, grain boundary mobility, anisotropy.]

Presented at the 91st Annual Meeting of the American Ceramic Society, Indianapolis, IN, April 25, 1989 (Basic Science Division, Paper No 65-B-89).

* Now at National Institute of Standards and Technology, Gaithersburg, MD 20899

+Member, American Ceramic Society.

Research supported by the Director, the Office of Energy Research, Office of Basic Energy Sciences, Materials Sciences Division of the U.S. Department of Energy under Contract No. DE-AC03-76SF00098.

Table of Contents

Introduction

Grain growth in alumina has been the subject of extensive investigation for more than thirty years. In general, two experimental approaches have been used to investigate grain boundary migration characteristics. In the first, large seed crystals have been introduced into a powder compact [1,2], or bonded to an already densified compact [3]. The work focussed on identifying the effect of MgO on grain growth rates; anisotropy of seed growth was not a primary concern. More recent work utilizing this approach has focussed on the effects of an intentionally incorporated liquid phase on the growth rate and morphology of the seed crystal [4,5]. The second approach has focussed on measuring the growth characteristics of the average grain in a polycrystalline matrix. Recent work [6,7] has helped to clarify the influence of, and interaction between, a glassy phase and MgO-dopant on grain growth in alumina.

There are, however, situations in which knowledge of only the average behavior is inadequate, and the factors that affect the anisotropy of grain growth, and control not only the size and size distribution, but also the evolution of the grain shape and grain shape distribution are of interest. For example, in considering the fracture strength of a ceramic, the edge length of large nonequiaxed (possibly abnormal) grains is of interest, because these edges may provide preferred sites for fracture initiation [8]. If aluminas with strong R-curve behavior are desired, it is advantageous to produce a matrix with columnar or platelike grains, to reinforce crack bridging in the crack wake [9]. For fabrication of such materials, knowledge of the factors that promote anisotropic grain growth is necessary.

In this study, the two aforementioned approaches were combined. Measurements of the average grain growth rate in theoretically dense undoped and MgO-doped polycrystalline alumina, and of the growth rate of oriented (basal and prismatic plane) sapphire seeds into both

an undoped and a MgO-doped polycrystalline matrix were performed. The experiments were designed to minimize the potential effects of a liquid phase and pore drag [10,11] on grain growth characteristics, and thereby allow a meaningful comparison between normal grain growth in, and grain boundary migration of an abnormal grain into, dense material with the same composition, but under the influence of different driving forces, and with differing constraints imposed on the grain boundary misorientation.

The observed (normal and abnormal) grain growth kinetics can be interpreted in terms of a driving force dependent grain boundary mobility-grain boundary energy product, $M_b\gamma_b$. Notably, the driving force dependencies for the $M_b\gamma_b$ product for normal matrix grains and abnormal grains differ. The growth behavior of oriented seeds suggests a strong interplay between interface crystallography and structure, the nature of solute-boundary interactions, and the resulting uniformity of growth. Observations of twin formation enhanced grain growth, a phenomenon invoked by Handwerker [12] as a vital element in the promotion of abnormal grain growth, underscore the importance of interface crystallography. Collectively, the findings have implications with respect to the development of anisotropic microstructures, and the nucleation and sustained growth of abnormal grains.

Experimental Procedure

Polycrystalline, pore-free, undoped and 250 atomic ppm MgO-doped aluminas were produced by a method combining hot pressing and subsequent hot isostatic pressing [10,13]. This procedure assures the attainment of theoretical density in specimens while preserving a small grain size (5.6 μm for undoped alumina, 3.1 μm for MgO-doped alumina) and a low impurity content (Table I).

Undoped alumina[1] was hot pressed at 1410°C for 2 h under a pressure of 35 MPa, using a boron nitride[2] coated graphite die and boron nitride spacers[2]. This yielded material with a relative density of 99.4 %. Subsequently, hot isostatic pressing at 175 MPa for 1 h at 1500°C was used to complete densification.

The doped material was produced by mixing alumina powder[1] with sufficient double distilled water-$Mg(NO_3)_2 \cdot 6H_2O$ solution to introduce 250 atomic ppm MgO. Mixing was performed in a Teflon® beaker. The mixed powders were dried at 80°C, and subsequently calcined for 2 h at 600°C. The powder was lightly crushed with a Teflon® rod before loading into the hot pressing die. For this material, hot pressing was performed at 1375°C for 50 min using 35 MPa pressure. This yielded a specimen with a density of 98.4%. Hot isostatic pressing for 1 h at 1500°C at 175 MPa pressure again produced a theoretically dense material.

Slices were cut from the center of each of the samples and polished to a 0.25 μm finish. These were subsequently hot pressed against either a-plane $\{11\bar{2}0\}$ or c-plane {0001} sapphire[3] (1375°C for 1 h at 15 MPa). The final hot-pressed samples had dimensions of 2 x 9 x 18 mm. These were cut into small bars, cleaned with acetone, ethanol, and distilled water, and embedded in a powder of identical composition in a high-purity alumina crucible. Subsequently, heat treatments were performed at 1600°C in air with tempering times from 2.5 h to 100 h. After this step, a 50 to 100 μm-thick layer of material was removed, the specimens were polished, thermally etched (1 h at 1400°C for MgO-doped alumina, 2 h at 1400°C for undoped alumina), and examined using scanning electron microscopy.

---

[1]Sumitomo, A-HPT-F, New York

[2]Union Carbide, Cleveland, OH, HCM boron nitride powder and HBC boron nitride rod.

[3]Adolf Meller Company, Providence, R.I.

The average grain size $\overline{G}$ in the polycrystalline alumina was obtained using the linear intercept method [14]. $\overline{G}$ is equal to 1.5 $\overline{L}$, where $\overline{L}$ is the average linear intercept. At least 200 grains were measured for each sample. Grain boundary migration rates of the sapphire seeds were obtained by measuring the position of the sapphire-polycrystal interface after various tempering times relative to the initial interface position as marked by reference channels. These channels were etched into the sapphire prior to bonding [10,11,13] and served as huge, crack-like pores. At the onset of motion, the sapphire alumina interface separated from the reference channel, as illustrated in Figure 1. This technique allowed an accuracy of ±0.5 μm in determining the displacement of the original sapphire-polycrystalline alumina interface during annealing [10,13]. Following each anneal, the grain boundary advancement was measured at at least 50 positions along the interface.

Results

Microstructures of both the undoped and the MgO-doped alumina are shown after various anneal times at 1600°C in Figures 2a-d and 3a-d, respectively. The undoped alumina developed grains that appear columnar in cross sections. The incidence of facetted grain boundaries increased with anneal time, however, not all grains appeared to be susceptible to this tendency to develop a more anisotropic grain shape. These changes in grain morphology were accompanied by the creation of microcrack-like voids at triple points adjacent to elongated grains. Such pores appeared predominantly in undoped alumina after heat treatments exceeding ≈40 h at 1600°C. Since pore drag may have affected the grain growth kinetics in these (undoped) samples during portions of the anneal exceeding 40 h, only the results of grain size measurements from anneals of shorter duration are included.

Plots of average grain size versus anneal time for both the undoped and the MgO-doped alumina are presented in Figure 4a,b. These data were fitted to a grain growth law (correlation factor >0.96) of the form

$$\overline{G}^3 - \overline{G}_o^3 = Kt \qquad [1]$$

where G_o is the initial grain size, t the anneal time in seconds, and K is a constant. K for the undoped alumina was found to be 5.16×10^{-20} m^3 s^{-1}; for the MgO-doped alumina K = 1.28×10^{-20} m^3 s^{-1}.

Micrographs of polycrystal-single crystal interfaces are presented in Figure 5a-d. The growth front of basal plane ({0001}) sapphire seeds remained nearly planar, both macroscopically and on the scale of the grain size, during growth into both the undoped and the MgO-doped material, and displacements were uniform. In contrast, the growth of the prismatic plane ($\{11\bar{2}0\}$) sapphire seed into undoped alumina was highly nonuniform; growth front displacements varied by as much as a factor of 20 along the interface. At some positions the growth rate of the seed into the undoped polycrystalline matrix was as high as 10 μm/h at 1600°C, much higher than that for the growth of the basal plane seed into undoped alumina. For prismatic plane seed growth, MgO-doping had a pronounced effect on both the nonuniformity and the growth rate, resulting in a much more uniform advancement, and a reduced advancement rate, similar to that for basal plane seeds into doped alumina. For prismatic plane sapphire seeds, the seed/matrix interface was not planar at the grain size scale, but instead, appeared to be uniformly curved between intersecting matrix grain boundaries.

Grain boundary migration data for the three sapphire seed-polycrystalline matrix combinations characterized by uniform growth are shown in Figure 6a. Error bars are given for

the growth of the basal plane seed into the undoped alumina. The spatial variability in the displacement for the other two cases was similar. For these combinations, seed growth data were fitted (correlation factor >0.97) to a growth law of the form

$$\overline{\Delta G}^2 = Lt \qquad [2]$$

where $\overline{\Delta G}$ represents the advancement of the sapphire after time t, and L is an empirical constant. The data are presented in this format in Figure 6b. The constant L was found to be 4.9×10^{-16} m^2/s for basal plane sapphire growing into the undoped matrix. The growth of basal plane sapphire into the MgO-doped matrix was characterized by a value for L of 36.5×10^{-16} m^2/s, and the growth of the prismatic plane into the MgO-doped alumina by a value of 38.8×10^{-16} m^2/s.

The data for growth of a prismatic plane seed into undoped alumina are presented in Figure 7. Two features are noteworthy. First, migration is nonuniform, and this, rather than measurement error, contributes to the large "error" bars. A comparison with Figure 6 shows that the variability is much larger than that for the growth of the basal plane seed into chemically and microstructurally equivalent material. Second, the interaction between the seeds and the dopant is seed orientation dependent. In comparing the displacement behavior of basal and prismatic seeds growing into undoped versus MgO-doped material, the differences in matrix grain size, and thus, the driving force acting on the seed must be taken into account. As discussed in a later section, the increase in the average displacement for the basal plane seed is largely due to this driving force difference. However, despite the increased driving force, the average displacement for the prismatic plane seed into the doped material appears to be less than that into undoped material. Thus, in this case there is a more significant effect of the dopant on the grain boundary mobility.

The preceding results suggest an effect of grain boundary structure on grain boundary migration rates, and a relationship between grain boundary structure and the effect of a dopant. An additional example of crystallographically induced changes in migration behavior is provided in Figure 8. The zone of enhanced grain growth, as seen to the right of the crack in Figure 8, is associated with the appearance of rhombohedral twins in the vicinity of the lithographically introduced interfacial cracks. These twins were observed only in samples in which MgO-doped polycrystalline alumina was bonded to basal plane sapphire. All twins resulted in a zone of accelerated growth of the sapphire into the polycrystalline matrix. Preliminary measurements indicate that the migration rate in this zone is approximately twice that for the untwinned basal plane.

Discussion

Several topics will be addressed. First, observations pertaining to the evolution of facetted grains and intergranular porosity as a result of anisotropic grain growth rates will be discussed. The empirical grain growth law and constants which describe the evolution of matrix grains are compared with those obtained in previous studies, and a framework for understanding the implications of the grain growth law is suggested. Seed growth data are evaluated and suggest, as does the growth data for matrix grains, that the grain boundary mobility-grain boundary energy product is an apparent function of driving force. The driving force dependencies of the grain boundary mobility-grain boundary energy product of matrix and abnormal grains are compared, and the implications of their being different on microstructural evolution are discussed. Finally, the observations of twin enhanced grain boundary migration are addressed.

Morphological Evolution

The most closely related studies of matrix grain growth kinetics in dense undoped and MgO-doped alumina are those by Bennison and Harmer [6,7]. Grain growth kinetics as well as grain morphology were sensitive to the amount of glassy phase present. In samples containing ≈1000 ppm metal impurities, grain growth in the undoped alumina produced a very anisotropic grain structure [6], while grains in the undoped alumina containing no glassy phase appeared equiaxed [7]. In these studies, grain growth anneals were ≤10 h [6], and ≤7 h [7] in duration, and the maximum average grain sizes attained were of the order of 15 μm and 22 μm, respectively.

In our work, the development of elongated grains in undoped alumina initiated after approximately 10 to 20 h of annealing, and in the average grain size range of 11 to 17 μm. We suggest that the degree of facetting during grain growth is a consequence of a competition between atomic transport perpendicular to the grain boundary which results in grain growth, and thereby a decrease in grain boundary ***area***, and atomic transport parallel to the grain boundary, which results in grain facetting, and thereby a decrease in grain boundary ***energy***. Specifically, when the grain size is small, the chemical potential difference between atoms in opposing grains at the interface is large, and transfer of mass across grain boundaries dominates the morphological evolution of the grain assembly. When the grain size has increased sufficiently, decreases in free energy brought about by facetting assume greater importance, and lead to the development of facetted grains and anisotropic grain growth behavior.[1]

[1] A similar transition between mass transport processes that produce global changes in morphology and those that result in the development of equilibrium shapes is evident during the morphological evolution of pores with initial shapes that are far from the equilibrium Wulff shape [13].

A facetting transition can also be brought about by glassy phase accumulation at the grain boundaries as the average grain size increases. At this point, we cannot distinguish which of the two processes leads to the observed facetting transition. We note, however, that the development of facetted grains appears to initiate at a significantly larger grain size than that reported by Bennison and Harmer in their initial study, and consequently, the glassy phase content of our samples appears to be less than that in their Linde A derived compacts.

For samples containing facetted grains, cracklike pores along grain faces, as well as more equiaxed pores at triple junctions between facetted interfaces, developed during annealing. We use the term desintering to describe this process of pore formation, and distinguish it from bloating or swelling, terms used to describe a process of pore nucleation due to internal oxidation of carbon impurities [15]. In contrast to bloating, desintering is not the result of a chemical interaction between the sample and the furnace atmosphere. It appears to be a consequence of reducing the net interfacial free energy of the specimen through the selective formation of pores. It is apparently energetically favorable to nucleate pores with low energy surfaces, if such pore formation facilitates the formation of low energy (facetted) grain boundary segments. This proposition that pore formation is not associated with a chemical reaction was verified by heating the undoped alumina in an atmosphere where no bloating occurs (argon gas gettered by Zr-Ti chips). Desintering occurred in the same manner as in samples tempered in air. At significantly coarser grain sizes, thermal expansion mismatch induced cracking of samples can occur during cooling, however, we do not believe that this is responsible for the development of pores in these specimens.[1]

[1]Microcracking due to thermal expansion mismatch is normally observed in alumina compacts in which the grain size is in the range of 50-60 μm. The cracks also have a small crack opening displacement and tend to extend over several grain diameters. The pores formed during desintering are more localized at three grain junctions.

The microstructures obtained as a result of anisotropic grain growth, interfacial facetting, and desintering (see Figure 2d) appear very appealing as potential high toughness single phase microstructures. Elongated grains can serve as bridges to apply closure forces in the crack wake [9], and pores at triple points concentrate local stresses at grain boundaries and prevent intergranular failure. In contrast, the microstructure of the MgO-doped alumina is equiaxed, consistent with results of other investigations [6,7,13].

Matrix Grain Growth Kinetics

Results for the empirically obtained grain growth constant K are compared with the results obtained in previous studies [6,7] in Table II. The value of K for the MgO-doped material obtained in this study is almost identical to that obtained by Bennison and Harmer in their higher purity material [7], and a factor of three less than that reported for MgO-doped material prepared from lower purity Linde A powder. In contrast, the ***ratio*** of $K_{undoped}/K_{MgO\text{-}doped}$ in the present study was approximately 4, and similar to that obtained by Bennison and Harmer in their lower purity materials [6]. The value of K for the undoped material is a factor of ≈3.4 lower than that obtained by Bennison and Harmer in their lower purity material [6]. Despite the good agreement obtained for MgO-doped materials, this disparity raised concern over contamination.

The Ca content of the powders used by Bennison and Harmer in their two studies is estimated as between 10 and 30 ppm for the Linde A powder [6] and as <0.5 ppm for the higher purity Sumitomo powder [7]; these values define lower limits on the calcium content in their dense compacts since contamination will occur during handling. Our chemical analysis indicated a Ca content of ≈10 ppm in the compact after densification was completed.

Although it is possible that our compacts contain more Ca than the higher purity specimens prepared by Bennison and Harmer, it is unlikely that they contain more Ca than the Linde A derived samples, since a higher concentration of glass formers should have resulted in the formation of facetted microstructures at fine average grain sizes (≤9 μm) [6]. Thus, the difference in the behavior of the undoped specimens is puzzling.

The results of grain growth experiments are often expressed in the form

$$\overline{G}^n - \overline{G}_o^n = Kt \qquad [3]$$

where $\overline{G}$ is the average grain size at time t, $\overline{G}_o$ is the average grain size at time t = 0, and n is the grain growth exponent. The normal grain growth rate can also be related to the grain boundary velocity V, the grain boundary mobility M_b, and the driving force for grain growth F_b via the relationship

$$\frac{d\overline{G}}{dt} = 2V = 2M_bF_b \qquad [4]$$

Since Eq. 3 is simply the integrated form of Eq. 4, it is evident that the grain growth exponent is dependent upon the grain size dependence of the mobility-driving force product. When $\overline{G}_o \ll \overline{G}$,

$$V = M_bF_b = \frac{1}{2}\frac{d\overline{G}}{dt} \approx \frac{K}{2n\overline{G}^{n-1}} \qquad [5]$$

For dense, pure, single-phase material, the grain boundary mobility is assumed to be independent of the grain size, and the driving force for growth is normally taken to be inversely proportional to the average grain size. For steady-state solute drag limited grain boundary migration in the low velocity limit, the grain boundary mobility is approximately

inversely proportional to the bulk solute concentration and independent of the grain size, and the driving force is again assumed to be inversely proportional to $\overline{G}$. For both cases, a grain growth exponent of n = 2 is predicted.

The normal grain growth data obtained in the present study fits a cubic growth law. In the context of Eq. 5, this requires that the mobility-driving force product be inversely proportional to $\overline{G}^2$. Several explanations have been proposed to account for the frequent occurrence of cubic grain growth kinetics in ceramics [16,17].

Progressive thickening of a continuous intergranular liquid phase leads to a driving force for growth that is inversely proportional to $\overline{G}^2$. If all impurities in our specimens are assumed to be incorporated into a glassy boundary phase, we estimate that a continuous 0.5 nm-thick grain boundary phase would exist at a mean linear intercept of ≈10 μm, or equivalently at an average grain size of 15 μm. The grain growth kinetics are cubic even at finer grain sizes, and facetting is not observed. Consequently, we do not consider a glassy phase to be a key factor in dictating the observed normal grain growth kinetics, although possible effects of glassy phases at selected boundaries are possible.

A cubic growth law can be explained if the mobility is assumed to be inversely proportional to the grain size. Brook has proposed that for solutes that segregate strongly, the bulk solute concentration will become dependent upon grain size at sufficiently fine grain sizes, and a cubic growth law would result [18]. However, at even finer grain size, in the limit of intrinsic grain boundary migration, the grain boundary migration rates should be insensitive to solute content, while at sufficiently coarse grain sizes, steady-state solute drag limited behavior should become dominant. Thus, in principle, a transition from parabolic to cubic to parabolic grain growth, accompanied by potentially very large shifts in growth rate,

should take place when a sufficiently wide range of grain size is spanned. No evidence for transitions in growth law was found in the present study, however, the average driving force for grain growth varied by only a factor of three for the undoped material, and by only a factor of five for the doped material. If segregation phenomena of the type proposed by Brook plays a role, it would not appear to be associated uniquely with segregation of MgO; a cubic grain growth law is observed for both MgO-doped and undoped alumina.

The role of grain boundary structure has been considered by several authors. Grain boundary migration models that take into account effects of the grain boundary plane [19], or of the grain boundary plane and misorientation [20] on the structure of the grain boundary have been developed. The migration rate is sensitive to the density and height of ledges and kinks, or steps associated with grain boundary dislocations. Depending upon the driving force dependence assumed for the transfer site density, migration rates with linear, square, and even exponential dependencies on driving force have been predicted. During grain growth, changes in the driving force dependence of the mobility-driving force product can occur, leading to changes in the grain growth exponent. More recent computer simulations of grain growth propose a value of n close to 3 [21,22], and a stochastic model of grain growth provides a wide range of n values depending upon the kink density and assumed half-life of the kinks [23].

If grain boundary structure arguments are invoked to account for the observed growth kinetics, the grain size dependence of the mobility can be attributed to a progressive decrease in the areal density of the grain boundary sites at which mass transfer occurs. The development of facetted microstructures in undoped alumina would appear to be consistent with this assumption. In MgO-doped alumina, the driving force for the development of

facetted microstructures is apparently reduced, as evidenced by the persistence of equiaxed grain structures. In the doped material, the onset of facetting could then be shifted to a coarser grain size, although a decrease in kink/step density may still occur during grain growth. Increases in the anneal temperature may also reduce the driving force for facetting and thereby increase the grain size at which facetting initiates.

Kinetics of Seed Growth

Four combinations of seed crystal orientation and polycrystal dopant content were explored. For growth of prismatic and basal plane seeds into MgO-doped material, and for the growth of basal plane seeds into undoped alumina, the growth was sufficiently uniform that the average displacement, $\overline{\Delta G}$, was an accurate measure of the interface motion.

The difference between the rates at which a basal plane seed grows into MgO-doped and undoped alumina, evident in Figure 6, is primarily the result of a difference in the driving force for growth (the grain size in the undoped material is larger than that in the undoped material). Thus, in this particular case, the orientation of one of the two adjoining grains appears to dominate the migration characteristics.

For the prismatic plane sapphire seed, the nonuniform migration into undoped alumina indicates that the grain boundary migration characteristics are sensitive to local misorientation. The grain to grain variations in orientation along the growth front induce displacement variations that do not appear attributable solely to driving force variations along

the growth front.[1] With the addition of magnesia, the displacements are much more uniform, and the "average" velocity approaches a value close to that for a basal plane seed growing into the same doped matrix.

There appears to be an important effect of grain boundary structure on the nature of the interaction between the moving sapphire/alumina interface and a solute. Specifically, MgO additions appear to have little effect on the mobility of a basal plane seed, but have a strong homogenizing effect on the mobility of a prismatic plane seed. The difference in grain boundary structure imposed by the differing seed orientations appears to have no influence on the characteristics or rate of migration into an MgO-doped polycrystalline matrix.

There are also interesting differences in the growth interface morphology for the two seed orientations. In the case of the basal plane seed, the interface remains nearly planar at the grain size scale during growth into both undoped and MgO-doped alumina. Even when controlled-geometry pore arrays were introduced at the sapphire/alumina interface, and pore-boundary interactions led to some departure from planarity, the planar interface was reestablished shortly after pore-boundary separation occurred [11].

These observations appear to contradict findings of Kaysser et al. [4]. In their work, sapphire spheres growing into a MgO-doped, glass-free, polycrystalline alumina did not undergo facetting. However, these experiments were conducted at 1800°C, and at this higher temperature the driving force for facetting may be reduced. Moreover, in our work, the facetted plane did not need to develop during growth, but instead was present initially, and was simply maintained during migration.

[1] A comparison of the mobility in undoped alumina with that expected for intrinsic migration suggests that background impurities play an important role in determining migration kinetics in alumina. The variability in displacement may indicate differing tendencies for breakaway from background impurities.

In contrast to the basal plane seed, the prismatic seed exhibited curved grain boundary segments. This difference in curvature, and presumably, a corresponding difference in the density and height of ledge or steplike defects at the interface also did not appear to have any significant effect on the migration kinetics during growth into the doped matrix.

Comparison of Matrix Grain and Seed Growth Kinetics

To compare the matrix and seed growth kinetics, it is convenient to assume that the driving forces for both grain growth and seed growth have the same dependence on the average grain size. In the following discussion, an inverse dependence is assumed, and differences in the time dependence of the grain boundary velocity, are attributed to differences in the time (or grain size) dependence of the mobility.

For normal grain growth, the increase in the average grain size can be related to a statistically averaged boundary velocity, and thus in turn to an average product of a grain boundary mobility and a driving force for grain growth. The driving force is associated with a pressure difference across the interface, and is related to the curvature of the boundary. Hillert estimated the net driving force for growth of a grain of size G owing to curvature as

$$F = 2\eta\gamma_b\left(\frac{1}{G_c} - \frac{1}{G}\right) \qquad [6]$$

where η is $\approx$1.25, and G_c is a time-dependent critical grain size [24]. The average grain size is estimated as (8/9)G_c. Using this relationship between $\overline{G}$ and G_c, and an expression for the time dependence of G_c [24], one can deduce that

$$\frac{d\overline{G}}{dt} = \frac{M_b\gamma_b}{\overline{G}} \qquad [7]$$

Comparing Eq. 5 (with n = 3) and Eq. 7, we obtain

$$M_b\gamma_b = \frac{K}{3\overline{G}} \qquad [8]$$

This grouping of terms is particularly convenient because all terms on the right hand side are measured in the grain growth experiment.

Equation 8 is valid within the grain size range studied. Clearly, the $M_b\gamma_b$ product cannot increase indefinitely as the grain size decreases. Yan et al. [16] have estimated the intrinsic mobility for alumina as $\approx 5 \times 10^{-12}$ m^4/J•s at 1600°C. If Eq. 8 is assumed to be valid over a wide range of grain size, the intrinsic mobility would be exceeded in the undoped material at an average grain size below ≈ 0.008 μm, well below the grain size range studied.[1] More significantly, the maximum mobility in the current normal grain growth measurements ($\approx 6.8 \times 10^{-15}$ m^4/J·s for undoped alumina, $\overline{G} = 5.6$ μm) is nearly three orders of magnitude less than the predicted intrinsic mobility. Thus, significant effects of background impurities are indicated even within the undoped material, and differences in background impurity content can be expected to impact absolute rates of grain boundary migration in both undoped and doped materials. The grain size dependence of the $M_b\gamma_b$ product also implies a time dependence. If $\overline{G}_o$ is negligible in comparison to $\overline{G}$, then $M_b\gamma_b$ is proportional to $t^{-1/3}$.

For seed growth, the driving force for growth can be estimated as the total interfacial energy density of the sample, and is given by [16]

$$F = \gamma_b\left(\frac{2}{\overline{L}}\right) = \gamma_b\left(\frac{3}{\overline{G}}\right) \qquad [9]$$

[1]This estimate defines a strict lower limit on the grain size range over which the relationship could be valid. In practice, breakaway from background solutes would occur at a larger grain size.

Thus, for one-directional seed growth the grain boundary velocity can be expressed in the form

$$V = \frac{d\overline{\Delta G}}{dt} = M_b F_b = \frac{3M_b\gamma_b}{\overline{G}} \qquad [10]$$

For basal plane seed growth into MgO-doped and undoped alumina, and for prismatic plane seed growth into MgO-doped alumina, $(d\overline{\Delta G}/dt)(\overline{G})$ decreases with time. Differentiating Eq. 2 with respect to time, and comparing the result with Eq. 10 provides a relationship between the empirical constant L, the term $M_b\gamma_b$, the average grain size $\overline{G}$, and the average advancement of the seed, $\overline{\Delta G}$

$$M_b\gamma_b = \frac{L\overline{G}}{6\overline{\Delta G}} \qquad [11]$$

Inserting Eq. 1 and Eq. 2 into this relationship reveals that for seed growth $M_b\gamma_b$ is proportional to $\overline{G}^{-1/2}$. Equivalently, $M_b\gamma_b$ is approximately proportional to $t^{-1/6}$.

The $M_b\gamma_b$ products for both the polycrystals and the seeds are dependent upon the average grain size. The values of the $M_b\gamma_b$ products for several growth conditions are compared in Table III. The average grain sizes in MgO-doped alumina after 10 h annealing ($\overline{G}$ = 7.9 μm) and after 40 h annealing ($\overline{G}$ = 12.3 μm) were chosen to define the driving forces for growth. The results indicate that $M_b\gamma_b$ for undoped polycrystalline alumina is approximately a factor of four to five higher than $M_b\gamma_b$ for MgO-doped polycrystals, and for growth of basal and prismatic plane seeds into an MgO-doped matrix. Within the indicated grain size range and misorientation range investigated, MgO-doping leads to a nearly isotropic $M_b\gamma_b$ product. As suggested previously, MgO-doping has little effect on $M_b\gamma_b$ for the basal plane seed.

A comparison of the grain size and time dependencies of the $M_b\gamma_b$ products for seeds and matrix grains reveals that $M_b\gamma_b$ for the seed does not decrease as rapidly with time as $M_b\gamma_b$ for the average grain boundary in the polycrystalline matrix. The ratio of M_b for the seed and the matrix grains can be expressed in the form

$$\frac{(M_b)_{seed}}{(M_b)_{matrix}} = \frac{L^{1/2}\overline{G}^{1/2}}{2K^{1/2}} \qquad [12]$$

Thus, for the conditions explored, the mobilities (and $M_b\gamma_b$ products) for the seed and matrix grains are generally different, and the ratio of the mobilities changes with time.

The results of Monahan and Halloran [2] and those of Kinoshita [3] also indicate differing grain size and time dependencies for the mobilities of the undoped matrix grains and seeds growing into undoped material, however they differ from the results obtained in the present study. In Kinoshita's work, grain growth in the undoped matrix was described by an approximately cubic growth law, while the rate of seed growth into undoped alumina appeared to be independent of time, and therefore independent of driving force [3]. Monahan and Halloran observed a similar time-independent growth rate of the seed into undoped alumina [2]. In both cases, introduction of MgO led to a reduced rate of matrix grain growth and a decaying (driving force dependent) rate of seed growth.

Yan has considered the effect of misorientation related mobility differences on grain growth. A specific range of grain boundary misorientations were assumed to have a mobility ten times that characterizing average grains. The results of a computer simulation suggest that when the misorientation between a larger than average grain and one of its neighboring grains is such that is has a tenfold mobility advantage over other grain boundary segments, abnormal grain growth can result [25]. The development of a multimodal grain size

distribution was also predicted [26]. The effects of the degree of mobility anisotropy on the probability of initiating abnormal grain growth and on the grain growth exponent were unfortunately not considered [25,26].

Grest et al. have attributed anisotropy in the $M_b\gamma_b$ product solely to misorientation related variations in γ_b [27]. An anisotropy factor is introduced, which in essence defines the width of the misorientation range within which the energy of grain boundaries increases from zero (at 0° misorientation) to a value characteristic of the average high angle boundary. Their results indicate that as the anisotropy factor increases, the grain size distribution broadens and the grain growth exponent increases from 2.5 to 4. Since changes in the anisotropy factor reflect changes in the population density of boundaries with differing $M_b\gamma_b$ products, and not the range of $M_b\gamma_b$ values, these predictions are not directly relevant to the findings of the current study. We also note that despite the significant differences in $M_b\gamma_b$ anisotropy and the microstructures that evolve in undoped and MgO-doped aluminas, the grain growth exponent is unaffected.

If the difference in the time and grain size dependencies of the $M_b\gamma_b$ products is purely a consequence of misorientation related effects, then grain growth will be anisotropic (even in an initially uniform microstructure) when the grains are smaller than the size range investigated, and again when the grains become large. The results indicate that the variability in the $M_b\gamma_b$ ratio is more pronounced in the undoped material, and thus the effects of anisotropic growth should be more apparent. Since the average driving force for abnormal growth is approximately six times that for normal grain growth, the driving force ranges for seed growth and normal grain growth do no overlap, and it is not possible to preclude that the differences in migration kinetics simply reflect driving force differences.

Regardless of the origin of the variability in the $M_b\gamma_b$ ratio, the existence of the variability and a time and driving force dependence to the ratio has important implications with regard to normal and abnormal grain growth. Thompson et al. have considered the relative growth rates of normal and abnormal grains and indicate that if uniform grain boundary energy is the only factor affecting boundary motion, an abnormal grain will be reabsorbed by the growing matrix [28]. An additional assumption of a uniform grain boundary mobility is implicit in their analysis. The present results suggest that not only is there likely to be variability in the mobility, the seed to matrix $M_b\gamma_b$ ratio itself can be time dependent. If this observation is more generally valid, a reexamination and modification of existing models of abnormal grain growth may be warranted.

Crystallographic Aspects of Grain Boundary Migration

Several effects of grain boundary misorientation and grain boundary structure on solute-boundary interactions and grain boundary migration characteristics have already been discussed. We now focus on the observation that rhombohedral twins accelerate grain growth of the c-plane sapphire into the polycrystalline matrix. Anomalous grain growth in $BaTiO_3$ has also been related to an increased occurrence of twinning [29,30]. Recently, Handwerker has proposed a mechanism wherein twin formation is a vital element in the nucleation of abnormal grain growth [12].

We suggest that the twins nucleate as a result of the large stresses created by accumulating thermal expansion mismatch during heating from 1375°C, the bonding temperature, to the anneal temperature. The preferential appearance of twins in regions adjacent to lithographically introduced cracks suggests that their stress concentrating effect

facilitates the nucleation of rhombohedral twins. Twin formation is obstructed if preexisting interfacial cracks extend and relieve stresses, or if the grain size in the matrix is increased, which results in the initiation of cracks perpendicular to the interface and their extension into the polycrystalline material.

The rhombohedral twins apparently have a higher mobility than the c-plane sapphire-polycrystal interfaces. According to Handwerker, the additional ledges at the twin boundary accelerate grain growth which otherwise relies on ledge nucleation on the {0001} plane [12]. Thus, when grain growth is strongly related to the density of kinks and ledges on a grain boundary, the average transfer rate of an atom across the grain boundary can be influenced by processes and microstructural features that are located several microns from the actual transfer site.

Handwerker suggests that twinned grains with facet planes (particularly basal facets) intersecting the twin plane grow considerably faster than individual matrix grains. The factor of two increase in displacements suggests that there is indeed an enhancement of the mobility due to twinning, however, it is uncertain whether twofold enhancement would be sufficient to nucleate abnormal grain growth. Twinning at the sapphire/polycrystal interface was only observed when a basal plane seed was bonded to MgO-doped alumina. Conceivably, more significant enhancements may occur during growth into undoped material.

Summary

Grain boundary mobility-grain boundary energy products characterizing normal grain growth in dense, polycrystalline, undoped and MgO-doped aluminas were determined, and were compared to $M_b\gamma_b$ products characterizing the growth of large, oriented, single-crystal sapphire seeds into the same polycrystalline materials.

For grain growth in the polycrystalline matrix, the $M_b\gamma_b$ product is inversely proportional to the average grain size. Grain growth in the undoped alumina was observed to be anisotropic. This anisotropy became increasingly apparent with increasing grain size, and led to the development of microstructures which contain lathe-like (but not abnormal) grains. MgO-dopant reduces $M_b\gamma_b$ in polycrystalline alumina by a factor of approximately four, and reduces the anisotropy.

The $M_b\gamma_b$ product for seed growth is inversely proportional to the square root of the average grain size. Growth of prismatic plane seeds into undoped alumina is very irregular, and suggests strong effects of local grain boundary misorientation on $M_b\gamma_b$. The effect of MgO additions on seed growth is seed orientation specific. $M_b\gamma_b$ for basal plane seeds appears to be essentially independent of MgO content. In contrast, MgO additions appear to reduce the average $M_b\gamma_b$ product for a prismatic plane seed, and makes seed advancement more spatially uniform. Experiments utilizing seed crystals spanning a wider range of surface orientation may provide useful information on the relationship between local grain boundary misorientation, solute-boundary interactions, and resulting grain growth anisotropy.

The grain size and time dependencies of the $M_b\gamma_b$ products for matrix grains and abnormal seeds differ, and as a result, the relative growth rates of matrix and abnormal grains will vary with time. If this is a general feature, a re-examination of models of abnormal grain growth may

be warranted. Our findings suggest that larger than average grains may have a velocity advantage that increases with time. As a result, there may be a critical grain size for the initiation of abnormal grain growth. The anisotropy of grain growth can also be altered by the introduction of twins into the microstructure. Further work is necessary to establish whether such twins play an important role in the initiation of abnormal grain growth.

Acknowledgements

We acknowledge helpful discussions with S. J. Bennison, U. Eisele and C. A. Handwerker. We thank M. F. Yan for providing us with access to his unpublished work.

References

1. R. L. Coble and J. E. Burke, "Sintering of Ceramics," in Progress in Ceramic Science, Ed. J. E. Burke, Vol. 3, Pergamon Press, London, 197-251 (1963).
2. R. D. Monahan and J. W. Halloran, "Single-Crystal Boundary Migration in Hot-Pressed Aluminum Oxide", J. Am. Ceram. Soc., 62 [12] 564-567 (1979).
3. M. Kinoshita, "Boundary Migration of Single Crystal in Polycrystalline Alumina", Yogyo-Kyokai-Shi 82 [5] 295-296 (1974).
4. W. A. Kaysser, M. Sprissler, C. A. Handwerker and J. E. Blendell, "The Effect of a Liquid Phase on the Morphology of Grain Growth in Alumina," J. Am. Ceram. Soc., 70 [5] 339-343 (1987).
5. Y. Finkelstein, B. J. Hockey, S. W. Wiederhorn, J. E. Blendell and C. A. Handwerker, "Migration of Sapphire into Alumina", to be published in Sintering of Advanced Ceramics, ed. by C. A. Handwerker, J. E. Blendell and W. A. Kaysser, The American Ceramic Society, OH (1989).
6. S. J. Bennison and M. P. Harmer, "Effect of MgO Solute on the Kinetics of Grain Growth in Al_2O_3", J. Am. Ceram. Soc., 66 [5] C- 90-C-92 (1983).
7. S. J. Bennison and M. P. Harmer, "Grain Growth Kinetics for Alumina in the Absence of a Liquid Phase", J. Am. Ceram. Soc., 68 [1] C-22-C-24 (1985).
8. R. W. Rice, "Strength/Grain Size Effects in Ceramics," Proc. Brit. Ceram. Soc. (20) 205-207 (1972).
9. S. J. Bennison and B. R. Lawn, "Role of Interfacial Grain-Bridging Sliding Friction in the Crack-Resistance and Strength Properties of Nontransforming Ceramics," submitted to Acta Metall. (1988).
10. J. Rödel and A. M. Glaeser, "Pore Drag in Alumina," to be published in Sintering of Advanced Ceramics, ed. by C.A. Handwerker, J.E. Blendell and W.A. Kaysser, The American Ceramic Society, OH (1989).
11. J. Rödel and A. M. Glaeser, "Pore Drag and Pore-Boundary Separation in Alumina," J. Am. Ceram. Soc., this issue.
12. C. A. Handwerker, "Twin Formation in the Nucleation of Discontinuous Grain Growth in Alumina," to be published.
13. J. Rödel, "The Application of Controlled Interfacial Pore Structures to Pore Perturbation and Pore Drag in Alumina," Ph.D. Thesis, University of California, Berkeley, CA (1988).
14. R. L. Fullman, "Measurement of Particle Sizes in Opaque Bodies," Trans. AIME, 197 [3] 447-452 (1953).
15. S. J. Bennison and M. P. Harmer, "Swelling of Hot-Pressed Alumina," J. Am. Ceram. Soc. 68 [11] 591-597 (1985).

16. M. F. Yan, R. M. Cannon and H. K. Bowen, "Grain Boundary Migration in Ceramics"; in Ceramic Microstructures '76, Edited by R. M. Fulrath and J. A. Pask, Westview Press, 276-307 (1976)

17. R. J. Brook, "Controlled Grain Growth"; pp. 331-64 in Treatise on Materials Science and Technology, Vol. 9, Edited by F. F. Y. Wang, Academic Press, New York, 1976.

18. R. J. Brook, "The Impurity Drag Effect and Grain Growth Kinetics," Scripta Metall., 2, [7], 375-78 (1968).

19. H. Gleiter, "Theory of Grain Boundary Migration Rate," Acta Metall. 17, [7], 853-62 (1987).

20. C. M. F. Rae and D. A. Smith, "On the Mechanisms of Grain Boundary Migration," Philos. Mag. A, 41, [4], 477-92 (1980).

21. M. P. Anderson, "Computer Simulation of Grain Growth - I. Kinetics," Acta Metall., 32, [5], 783-791 (1984).

22. M. P. Anderson, G. S. Grest and D. J. Srolovitz, "Grain Growth in Three Dimensions: A Lattice Model," Scripta Metall. 19, [2], 225-30 (1985).

23. I-Wei Chen, "A Stochastic Theory of Grain Growth," Acta Metall., 35, [7] 1723-1733 (1987).

24. M. Hillert, "On the Theory of Normal and Abnormal Grain Growth," Acta Metall., 13, [3], 227-238 (1965).

25. M. F. Yan, "Microstructural Control in the Processing of Electronic Ceramics," Mater. Sci. and Eng., 48, [1], 53-72 (1981).

26. M. F. Yan and S. Lin, "Computer Simulation of Normal and Abnormal Grain Growth," unpublished research, (1979).

27. G. S. Grest, D. J. Srolovitz and M. P. Anderson, " Computer Simulation of Grain Growth - IV. Anisotropic grain boundary energies," Acta Metall., 33, [3], 509-520 (1985).

28. C. V. Thompson, H. J. Frost and F. Spaepen, "The Relative Rates of Secondary and Normal Grain Growth," Acta Metall., 35, [4], 887-890 (1987).

29. H. Schmelz and A. Meyer, "The Evidence of Anomalous Grain Growth Below the Eutectic Temperature in $BaTiO_3$ Ceramics," Ber. Dtsch. Ceram. Ges., 59, [819], 436-40 (1982).

30. D. F. K. Hennings, R. Janssen and P. J. L. Reynen, "Control of Liquid-Phase-Enhanced Discontinuous Grain Growth in Barium Titanate," J. Am. Ceram. Soc., 70, [1], 23-27 (1987).

APPENDIX I: AN ALTERNATIVE DRIVING FORCE FORMAT

There are two alternative means of expressing the driving force F for grain growth, and as a result, two means of expressing the mobility, M_b. In the formalism used in this paper, the driving force has the dimensions of energy per unit volume (e.g., J/m^3), or equivalently force per unit area (e.g., N/m^2). If the velocity is expressed in m/s, the mobility, the velocity per unit driving force, will have dimensions of $m^4/J \cdot s$, and the mobility-boundary energy product has dimensions of m^2/s. This formalism was used in the present paper because it is the more commonly used formalism in grain boundary migration papers in which mobilities and driving forces are considered.

The alternative formalism considers the driving force on a per atom basis, and multiplies F by the area of an atom, $\Omega^{2/3}$, where Ω is the atomic volume. The resulting driving force, F', has dimensions of energy per length or force. In the context of this latter formalism, equations 5 through 11 would be modified by a factor of $\Omega^{2/3}$ in the denominator. For this case, the mobility M_b' has dimensions of $m^2/J \cdot s$. The mobility-boundary energy product has the dimensions of a frequency, s^{-1}, and is related to the frequency of successful jumps. Relative values of $M_b'\gamma_b$ provides relative values of the grain boundary velocity at the same driving force, as in Table I-A; the product itself does not relate directly to the actual boundary velocity. The latter driving force and mobility formalism is used in the companion paper describing pore-boundary interactions in alumina.

Table I-A: Products of grain boundary mobilities and grain boundary energies ($M_b'\gamma_b$) for polycrystalline alumina and sapphire-polycrystalline alumina interfaces.

	polycrystals		interface		
	undoped	MgO-doped	basal/undoped	basal/doped	prismatic/doped
$M_b'\gamma_b$ for $\overline{G}$ = 7.9 μm (s^{-1})	28.5×10^3	7.1×10^3	3.9×10^3	5.3×10^3	5.5×10^3
$M_b'\gamma_b$ for $\overline{G}$ = 12.3 μm (s^{-1})	18.3×10^3	4.5×10^3	3.1×10^3	4.3×10^3	4.4×10^3

Tables

Table I: Impurity content of cations (in ppm) in polycrystalline alumina matrix

	undoped alumina	MgO-doped alumina
Mg	<10	200
Si	<30	<30
Ca	10	<10
Fe	<30	<30
Ni	10	--
Mn	<10	<10
Cu	<5	<5

Table II: Comparison of experimental rate constants K

Source	K in undoped Al_2O_3 ($m^3 s^{-1}$)	K in MgO-doped Al_2O_3 ($m^3 s^{-1}$)
single phase (reference 7)	5.17×10^{-19}	1.04×10^{-20}
with liquid phase (reference 6)	1.74×10^{-19}	3.90×10^{-20}
current work	5.16×10^{-20}	1.28×10^{-20}

Table III: Products of grain boundary mobilities and grain boundary energies ($M_b\gamma_b$) for polycrystalline alumina and sapphire-polycrystalline alumina interfaces.

	polycrystals		interface		
	undoped	MgO-doped	basal/undoped	basal/doped	prismatic/doped
$M_b\gamma_b$ for $\overline{G}$ = 7.9 μm (m^2/s)	2.18×10^{-15}	5.41×10^{-16}	2.98×10^{-16}	4.05×10^{-16}	4.18×10^{-16}
$M_b\gamma_b$ for $\overline{G}$ = 12.3 μm (m^2/s)	1.40×10^{-15}	3.47×10^{-16}	2.39×10^{-16}	3.26×10^{-16}	3.36×10^{-16}

Figure Captions

Figure 1: Large crack-like pore marking original position of interface after 30 h at 1600°C.

Figure 2: Grain structure of dense, undoped alumina after a) 0, b) 10, c) 20 and d) 100 h.

Figure 3: Grain structure of dense, MgO-doped alumina after a) 0, b) 7.5, c) 15, and d) 100 h at 1600°C.

Figure 4: Grain growth kinetics of undoped and MgO-doped alumina at 1600°C.

Figure 5: Interface between single crystal and polycrystalline alumina after 5 h at 1600°C (basal plane in a,b; prismatic plane in c,d; undoped alumina in a,c; MgO-doped alumina in b,d). The arrows indicate the original interface position.

Figure 6: Kinetics of boundary migration of basal plane sapphire into undoped and MgO-doped alumina, and prismatic plane sapphire into MgO-doped alumina.

Figure 7: Kinetics of boundary migration of prismatic plane sapphire into undoped alumina.

Figure 8: Example of (rhombohedral) twin formation enhanced grain growth at interface between basal plane sapphire and polycrystalline MgO-doped alumina. Sample was annealed for 30 h at 1600°C.

Figure 1

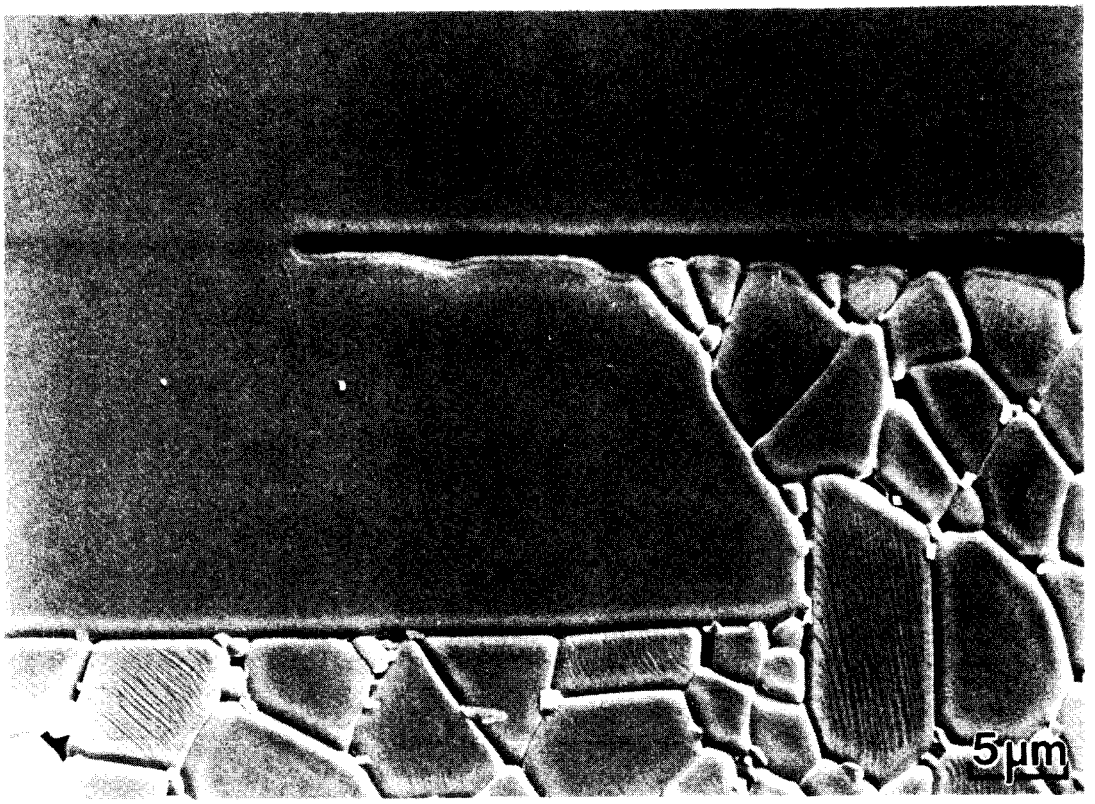

XBB 884-3499

Figure 2

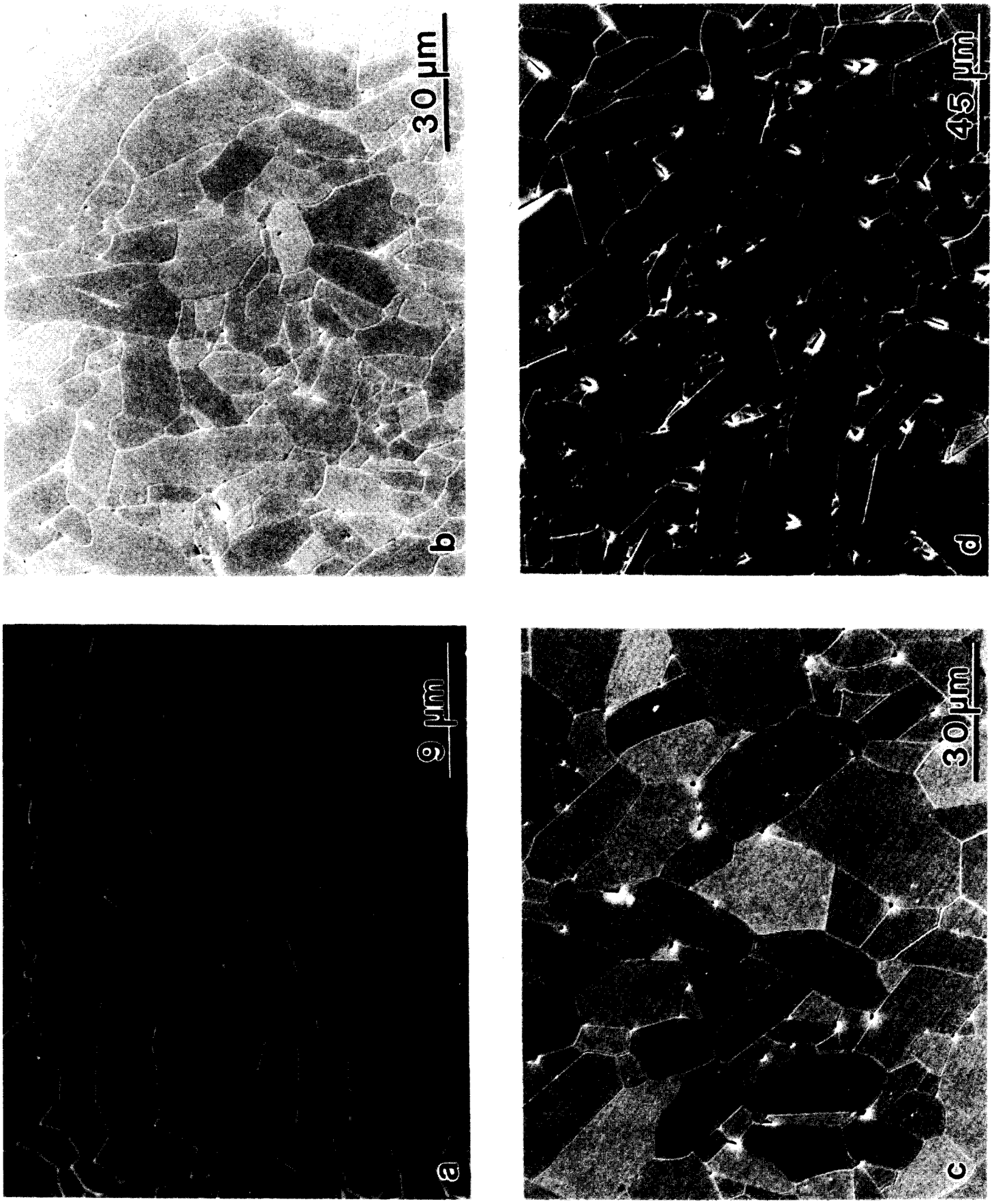

XBB 897-5870

Figure 3

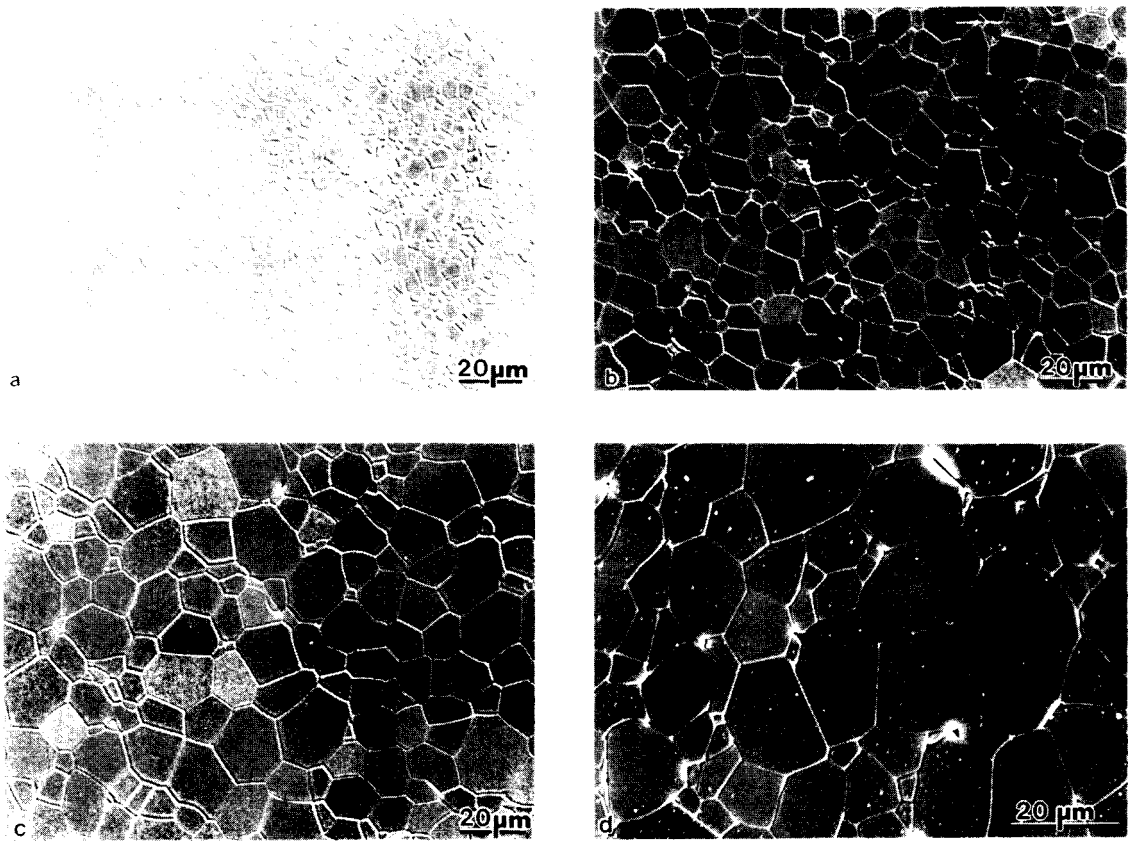

XBB 889-9106

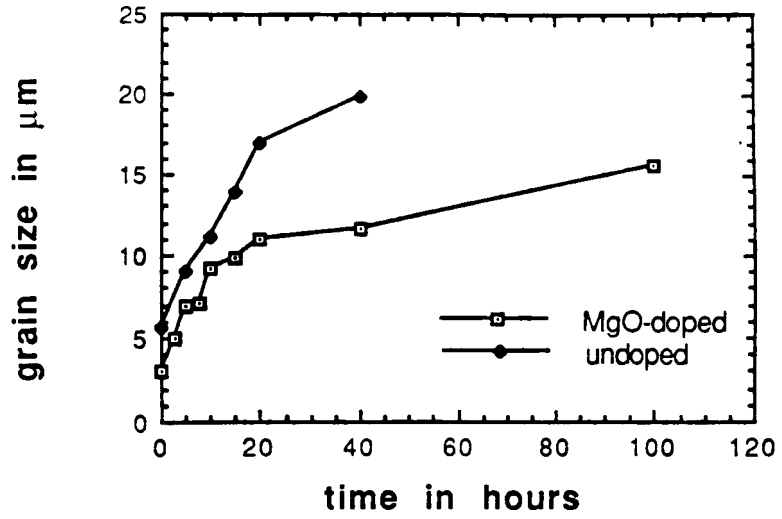
grain size in μm
25
20
15
10
5
0
0
20
40
60
80
100
120
time in hours
MgO-doped
undoped

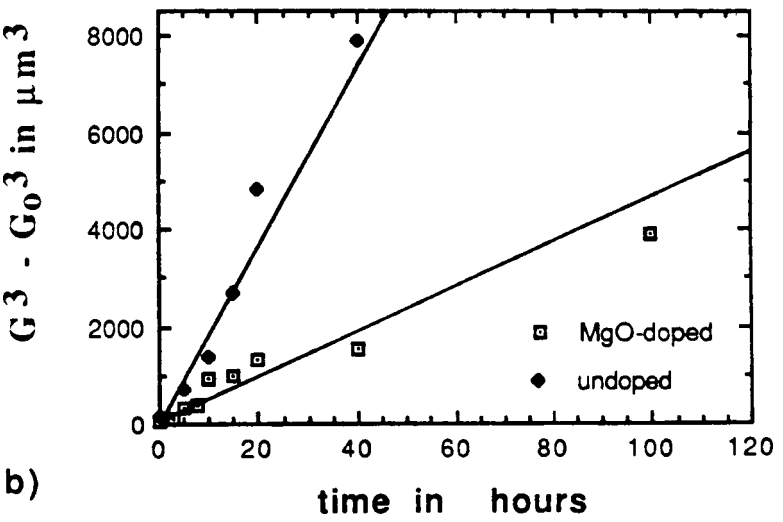
G3 - Go3 in μm3
8000
6000
4000
2000
0
0
20
40
60
80
100
120
time in hours
MgO-doped
undoped

b)

Figure 5

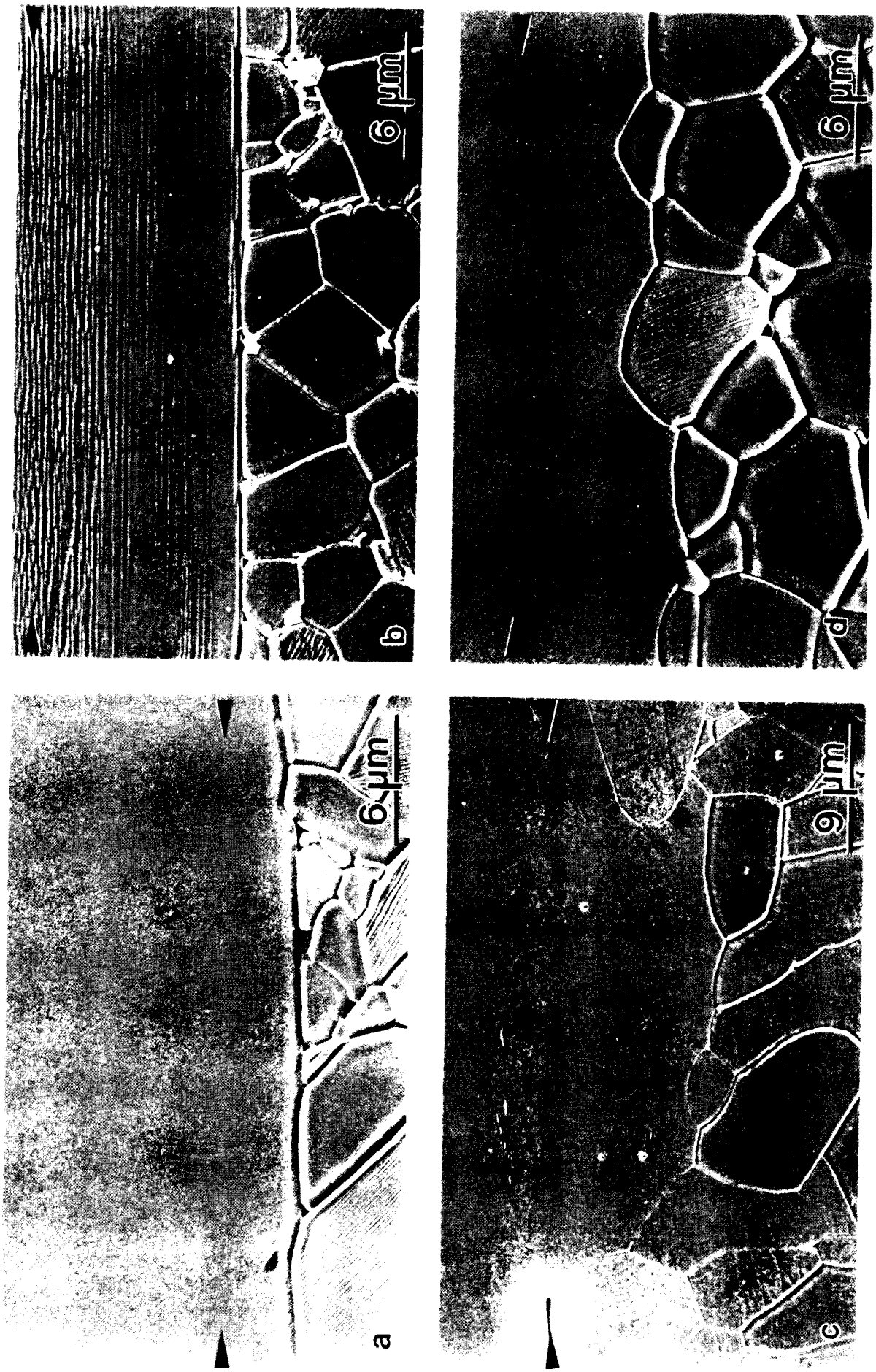

XBB 897-5871

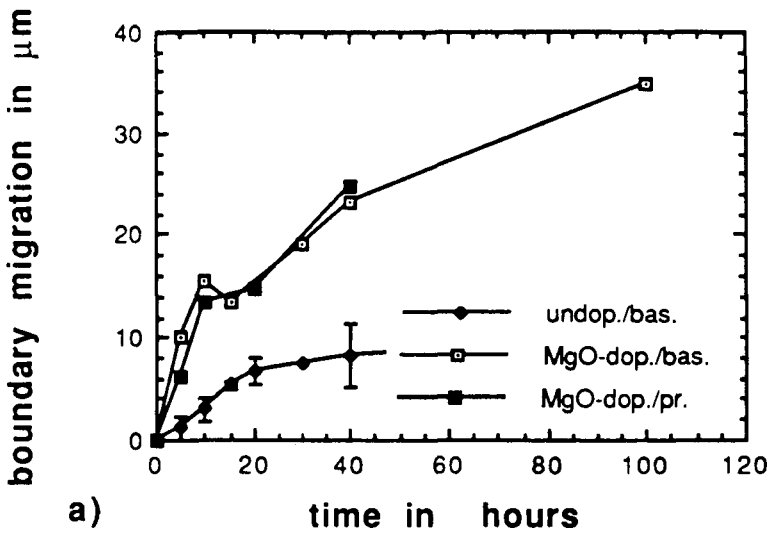

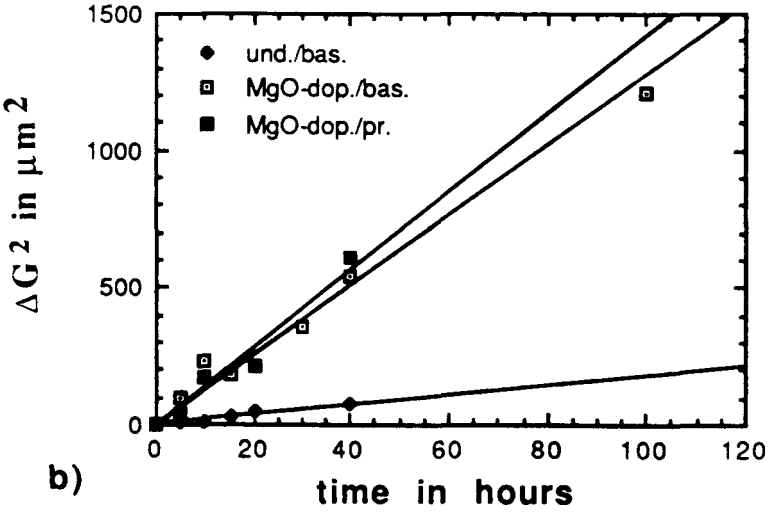

XBL 8910-3558

Figure 7

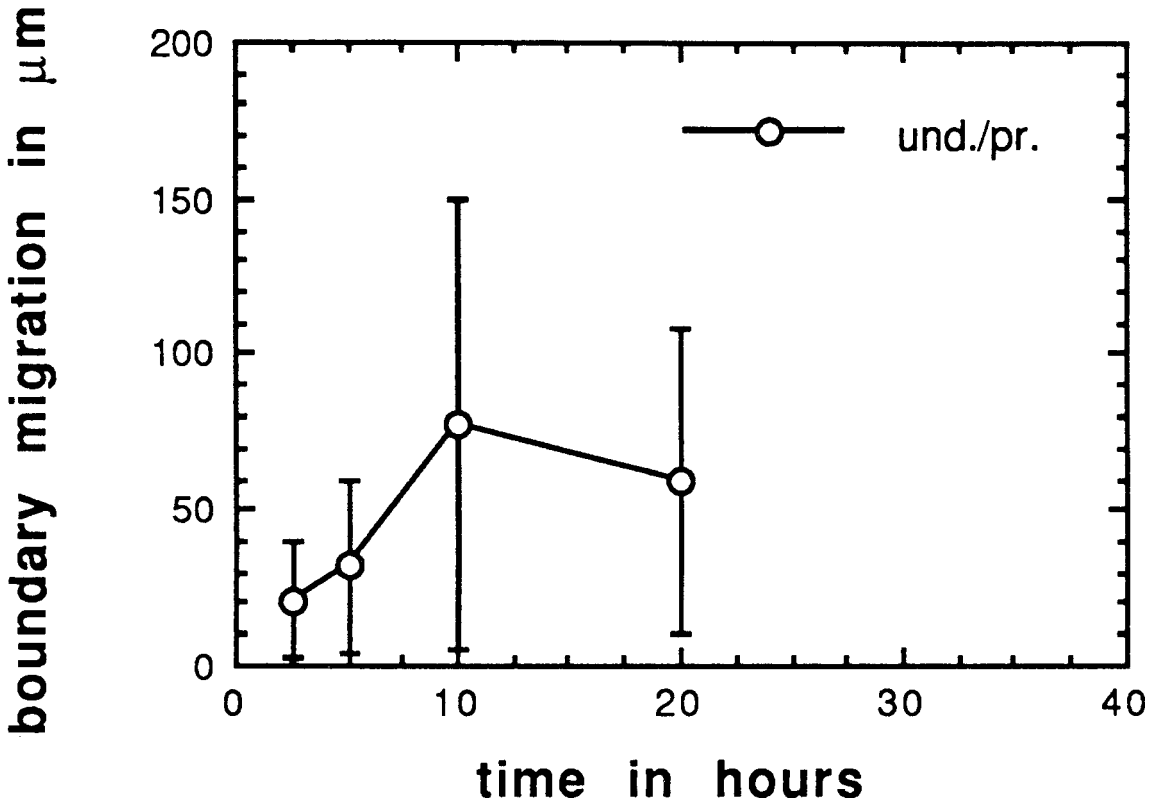

XBL 899-3218

Figure 8

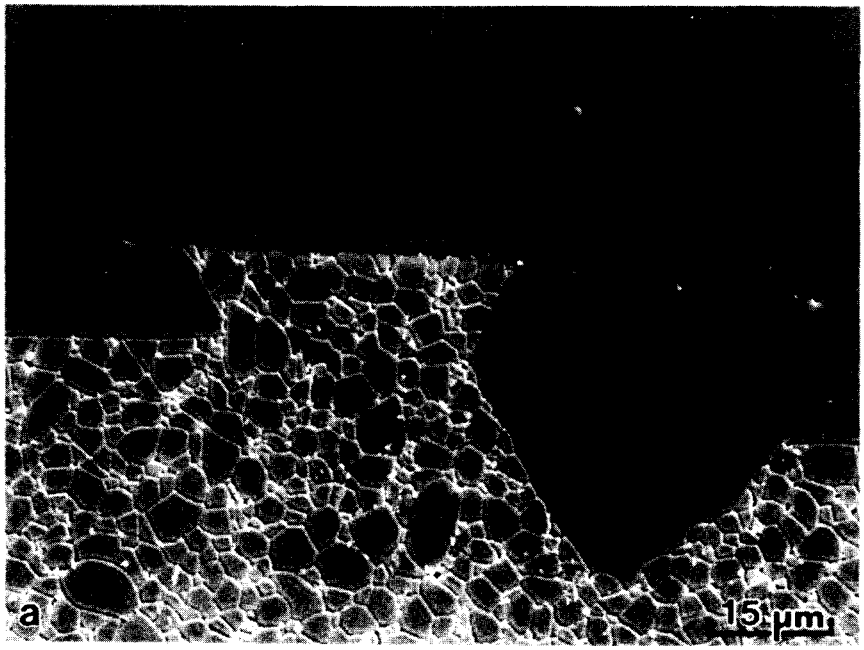

XBB 889-9101